AIP | Applied Physics Letters

Quantum-confined stark effect in localized luminescent centers within InGaN/GaN quantum-well based light emitting diodes

Suman De, Arunasish Layek, Sukanya Bhattacharya, Dibyendu Kumar Das, Abdul Kadir et al.

Citation: Appl. Phys. Lett. **101**, 121919 (2012); doi: 10.1063/1.4754079
View online: http://dx.doi.org/10.1063/1.4754079
View Table of Contents: http://apl.aip.org/resource/1/APPLAB/v101/i12
Published by the American Institute of Physics.

Quantum-confined stark effect in localized luminescent centers within InGaN/GaN quantum-well based light emitting diodes

Suman De,[1] Arunasish Layek,[1] Sukanya Bhattacharya,[1] Dibyendu Kumar Das,[2] Abdul Kadir,[3] Arnab Bhattacharya,[3] Subhabrata Dhar,[4] and Arindam Chowdhury[1,5,a)]
[1]*Department of Chemistry, Indian Institute of Technology Bombay, Powai, Mumbai 400076, India*
[2]*Department of Physical Chemistry, Indian Association for the Cultivation of Science, Jadavpur, Kolkata 700032, India*
[3]*Department of Condensed Matter Physics and Materials Science, Tata Institute of Fundamental Research, Homi Bhaba Road, Mumbai 400005, India*
[4]*Department of Physics, Indian Institute of Technology Bombay, Powai, Mumbai 400076, India*
[5]*National Center for Photovoltaic Research and Education, Indian Institute of Technology Bombay, Powai, Mumbai 400076, India*

(Received 8 May 2012; accepted 31 August 2012; published online 21 September 2012)

The nature of the polarization-field in disorder induced nanoscale potential fluctuations (radiative traps) within (In,Ga)N based quantum-well (QW) heterostructures remains ambiguous. Spectrally resolved photoluminescence microscopy has been utilized to probe the local polarization field by monitoring the extent of quantum-confined Stark effect (QCSE) in radiative trap centers spontaneously formed within an (In,Ga)N QW based light emitting diode. Interestingly, two distinct categories of nanoscale radiative domains, which arise from indium compositional and interface-morphology related fluctuations of the active layers, are found to have very different degree of built-in polarization fields. Screening of QCSE in indium-rich emission centers results in blue-shift of transition energies by up to 400 meV, significantly higher than that reported previously for group III-nitride based semiconductor heterostructures. A lack of correlation between the extent of QCSE and local indium mole-fractions suggests that size, shape, and strain of individual localization centers play a crucial role in modulating the local polarization field. © *2012 American Institute of Physics*. [http://dx.doi.org/10.1063/1.4754079]

Group III-nitride semiconductor based quantum well (QW) heterostructures are extensively used as active layers of solid-state light emitting devices, where the color and intensity of emitted light can be tuned by appropriate choice of alloy compositions and thickness of the QWs.[1,2] However, inhomogeneity in both the composition and morphology of the alloy exists in QW heterostructures, which results in spatial non-uniformities in energies and intensities of emanating photons. Such nanoscale disorders modulate the potential landscape of alloy layers resulting in spatial localization of carriers.[3,4] For instance, in $In_xGa_{1-x}N$ alloy based QW light emitting diodes (LEDs), carrier localization in spontaneously formed radiative traps is accredited to enhanced photoemission efficiencies despite the high density ($>10^9\,cm^{-2}$) of non-radiative dislocations.[2–5] Further, light emission characteristics of QW devices are severely affected by the existence of spontaneous and piezoelectric polarization induced electrostatic field along the usual growth direction (c-axis).[6] This built-in polarization field manifests itself in a red-shift of transition energies and reduction of emission efficiencies, commonly referred to as quantum confined stark effect (QCSE).[2] Due to obvious relevance for device applications, QCSE for InGaN/GaN heterostructures have been investigated in detail and is found to depend on crystal symmetry as well as the number, thickness, and composition of the active layers.[2,7–9] Interestingly however, the effect of nanoscale potential fluctuations on the local polarization field or vice versa, and its consequences on optoelectronic properties of InGaN based QWs remain unclear.

Disorder induced potential fluctuations enhance the radiative recombination (RR) efficiency by suppressing in-plane migration of carriers to non-radiative (NR) centers.[2,4] These spontaneously formed radiative trap centers, which span few angstroms to several tens of nanometers,[8,10] have different degree of local strain depending on their dimensions and compositions.[11,12] Thus, the local built-in polarization field in these nanoscale radiative domains is expected to be not only different from that of the alloy layer(s) but also inhomogeneous along lateral dimensions of the QWs. As a consequence, the extent of QCSE within individual emission centers is also anticipated to be non-uniform, which has a direct effect on the light emission characteristics of InGaN based QWs. Surprisingly, despite a few efforts, there is a dearth of unambiguous experimental evidence on the presence of QCSE within localized luminescent centers (LLCs) formed in QW heterostructures.[13,14]

Due to the presence of strong intrinsic polarization field (exceeding several MV/cm) in InGaN/GaN QWs, the degree of QCSE within nanoscale radiative domains is likely to be pronounced.[6,15,16] Further, for InGaN heterostructures, efficient potential traps formed within the QWs due to composition inhomogeneity and well-width fluctuation can be energetically distinct for a certain range of alloy layer thickness and compositions.[3–5] Using photoluminescence (PL) microscopy, it has been demonstrated that LLCs arising from both type of disorders can coexist in the same InGaN/GaN multiple QW LED sample; shallow traps are formed

a)Author to whom correspondence should be addressed. Electronic mail: arindam@chem.iitb.ac.in. Tel.: +91 22 2576 7154.

due to monolayer(s) fluctuations in interface morphology, while enhanced local indium mole-fractions lead to the formation of deep potential traps.[17,18] This opens up the possibility to interrogate the extent of QCSE in individual LLCs arising from either of the aforesaid mechanisms without altering other physical parameters. In this letter, using spectrally resolved PL microscopy, we have investigated a statistically relevant number of localized emission centers (along the polar [0001] plane) spontaneously formed within the green emitting InGaN QW-LED by varying photogenerated carrier density in the alloy layers. We demonstrate that the effect of inherent polarization field on the optoelectronic properties of individual localized luminescent centers, i.e., the extent of QCSE, is extremely diverse depending upon carrier localization mechanisms.

The epitaxial structures of the green-emitting LED used in this report were grown using metallorganic vapor phase epitaxy. The active layer consists of 5-period 4 nm thick $In_{0.22}Ga_{0.78}N$ alloy separated by lightly n-doped 10 nm thick GaN barrier layers. Ensemble (large-area) PL spectroscopy using 405 nm laser excitation showed a QW transition at ~2.6 eV. Spectrally resolved PL imaging was performed at 298 K in an epifluorescence configuration; a 488 nm line of an Ar^+ laser (excitation powers 3–1000 W cm^{-2}) was used to selectively generate carriers in the alloy layers in order to probe individual LLCs (Figure S1 in supplementary material[27]). Energy-mapped images were constructed by quantitatively superimposing PL intensity images (obtained using a CCD camera) of the same lateral area collected via two detection channels (band pass: 530–590 nm and 590–700 nm). Fluorescence lifetime imaging microscopy (FLIM) was carried out using a 470 nm pulsed laser diode with a 250 ps pulse-width operating at 10 MHz repetition rate. The lifetime-images and single spot time-resolved PL (TRPL) decay traces were obtained using time-correlated single photon counting technique. For further details, see supplementary material.[27]

Figure 1(a) shows an energy-mapped PL intensity image of the InGaN QW active layers at high excitation powers (500 W cm^{-2}). This pseudo-color optical image reveals the presence of several LLCs with varying intensities and emission energies, anisotropically located along in-plane dimensions. In this LED sample, the red-emitting LLCs, with transition energies at maximum excitation powers ($E_{Tr}^{P_{Max}}$) < 2.09 eV, arise due to increase of local indium mole-fractions with the alloy layers, while the green-emission centers (with $E_{Tr}^{P_{Max}} > 2.09$ eV) are related to disorders in interface morphology of the active layers[17,18] (see Figure S2 in supplementary material[27]). The excitation power (P_{Ex}) dependent PL intensity images of the same lateral-area (as in Figure 1(a)) in the absence of any emission filter is depicted in Figures 1(b)–1(d). Intriguingly, it is observed that only some of the LLCs show significant change in their emission efficiencies with decreasing power density. As opposed to the green centers (marked using arrows) for which the emission intensities scale proportionate to QW background, the red centers (marked using circles) display a dramatic reduction of light output efficiency with decreasing P_{Ex}. The spectral behaviors for a single red and a green emission center with increasing carrier density are shown in Figures 1(e) and 1(f). The entire PL envelope of the red emission center (Figure 1(e)) displays a continuous blue shift with increasing P_{Ex}, while the transition energy (E_{Tr}) of the green emission center (Figure 1(f)) remains essentially unchanged. Such disparity in power dependence of PL spectra between the green and red emissive traps is observed for a vast majority of LLCs at different spatial (in-plane) locations of this sample, as well as for two other multiple QW-LEDs having similar but not identical active layer thickness and alloy compositions.

A contrasting power dependence of the carrier recombination dynamics is also observed for the green and red emission centers. Representative FLIM images and TRPL decay profiles for individual red and green emission centers at three different pump-powers are shown in Figures 2(a) and 2(b). The sequence of power-dependent FLIM images (insets of Figures 2(a) and 2(b)) qualitatively portray that the PL lifetimes are significantly altered only for the red-emitting centers. Further, single-spot TRPL decay traces (Figure 2) obtained from individual LLCs demonstrate that the average PL lifetimes for red emissive traps decrease continuously (from ~40 to 20 ns) with increasing density of photogenerated carriers, while the radiative recombination dynamics within the green emission centers remain predominantly unaffected (~15 ns).

Figures 3(a)–3(c) depict the P_{Ex} dependence (from minimum power, $P_{Min} = 3$ W cm^{-2} to maximum power, $P_{Max} = 1$ kW cm^{-2}) of the optical properties for several arbitrarily chosen individual LLCs. The transition energies, relative integrated intensities, and spectral line-widths of individual LLCs were obtained by fitting each PL spectrum

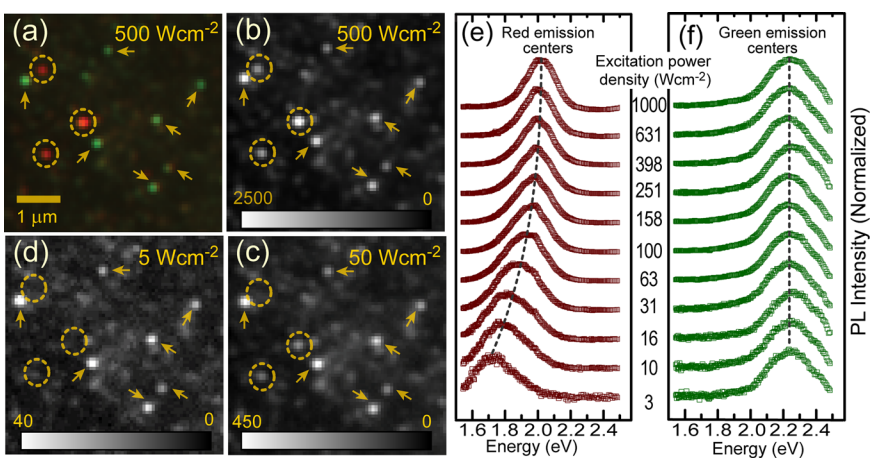

FIG. 1. (a) Energy-mapped (pseudo-color) PL intensity image of QWs for identification of green (arrows) and red (circles) emission centers, obtained at 500 W cm^{-2}. PL intensity images of the same lateral area in absence of emission filters at excitation power density (P_{Ex}) of (b) 500 W cm^{-2}, (c) 50 W cm^{-2}, and (d) 5 W cm^{-2} (calibration bars denote counts $pixel^{-1}$ s^{-1}). PL spectra of a single red (e) and green (f) emission center obtained P_{Ex} between 3 W cm^{-2} (P_{Min}) and 1 kW cm^{-2} (P_{Max}).

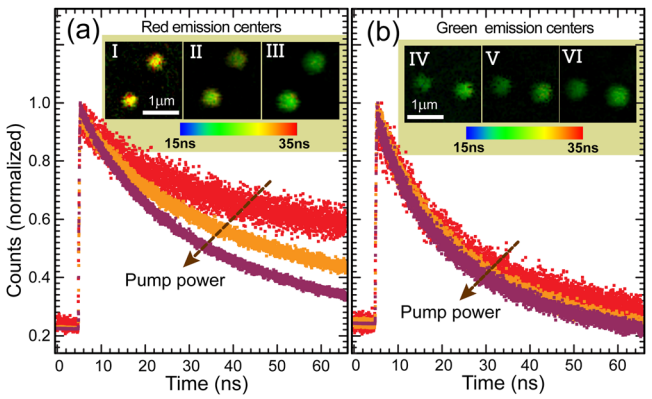

FIG. 2. Pump-power dependent single-spot TRPL decay traces for an individual (a) red and (b) green emission center, obtained by averaging the decay traces collected over tens of seconds. Arrows indicate increasing pump powers. The insets depict FLIM images of two different lateral areas of the QWs, each containing two (a) red or (b) green emission centers, as a function of increasing powers (I = IV < II = V < III = VI). The color-coded calibration bar represents the intensity weighted PL lifetimes for each pixel.

using a single Gaussian function (see inset of Figure 3(a)). For the red emission centers (Figures 3(a)–3(c), open symbols), all these parameters exhibit a systematic variation and saturation tendency with increasing P_{Ex}. The magnitude of such spectral changes is found to vary considerably from one emission center to another, uncorrelated with their respective $E_{Tr}^{P_{Max}}$ or $E_{Tr}^{P_{Min}}$. It is worth mentioning that the relative light output efficiency for the majority of red emission centers is found to be modest at low P_{Ex}, typically comparable or lower than that of the green centers (Figure 3(b)). However, with increasing carrier concentrations, red centers undergo more than three-fold enhancement of light output efficiency.

The systematic change in the optoelectronic behaviors for the red emission centers (Figures 1–3) demonstrates that compositional inhomogeneity induced potential fluctuations within the QWs lead to considerable reorganization of the band structure upon changing carrier densities. We ascribe this to coulomb screening of the local built-in field within

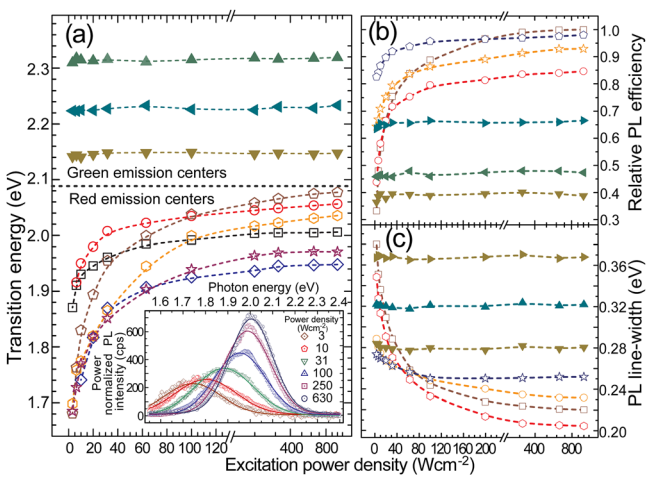

FIG. 3. P_{Ex} dependence of (a) transition energy, (b) relative PL efficiency, and (c) spectral line-width for several individual emission centers, obtained from single-Gaussian fits to each power normalized PL emission spectra (a, inset). The green (filled symbols) and red (open symbols) LLCs are discriminated using their $E_{Tr}^{P_{Max}}$ being above and below 2.09 eV (a, dotted line). Dashed lines are guide to visualize the trends.

these radiative nanoscale domains. It is noted that band-filling effect might have also resulted in blue-shift of E_{Tr}, except that such a phenomenon is accompanied by an energetically inhomogeneous broadening of the emission spectra.[14] However, a symmetric narrowing in spectral line widths is observed with increasing carrier density (Figure 3(c)), which effectively excludes band-filling effect as the probable cause.[13,14] Thus, the screening of QCSE within individual emission centers serves as the only viable mechanism for the observed power dependent blue-shift of the emission envelope with simultaneous enhancement of radiative recombination efficiencies.

The extent of the polarization field screening, which is directly related to the magnitude of this built-in field, is anticipated to vary from one center to another due to its dependence on the local compositions and well-widths.[7,19] Thermally activated background impurities, defects and dopants in the active layers are known to release free carriers in QWs, which suppress QCSE by screening the polarization charges at material interface.[16,20] Thus, at elevated temperatures, InGaN alloys with relatively low polarization field (such as those with narrow well-widths) are not expected to display significant QCSE screening with increasing carrier concentrations.[7,21] This also suggests that the effect of QCSE should not be dominant for radiative centers arising from interfacial roughness of thin wells. However, the built-in field can be quite large for nanoscale domains with indium mole-fractions higher than that of QW alloy,[19] which can fully, or in part, be compensated by photogenerated carriers leading to screening of QCSE.

Figures 1–3 suggest that the amount of local built-in field present within various individual emission centers is strongly dependent on the carrier localization mechanisms. This prompted us to probe the relative extent of QCSE within a statistically relevant number of LLCs, from various regions of this multiple QW-LED sample. The difference in E_{Tr} under screened and unscreened conditions, i.e., $\Delta E_{Tr} = E_{Tr}^{P_{Max}} - E_{Tr}^{P_{Min}}$, which serves as a measure of QCSE, is plotted in Figure 4 as a function of $E_{Tr}^{P_{Max}}$, for several hundred individual centers. This plot is clearly indicative of two distinct energetic regimes; ΔE_{Tr} is much more scattered for centers with $E_{Tr} < 2.09$ eV, while there is negligible change for those with $E_{Tr} > 2.09$ eV. This demonstrates the presence of an

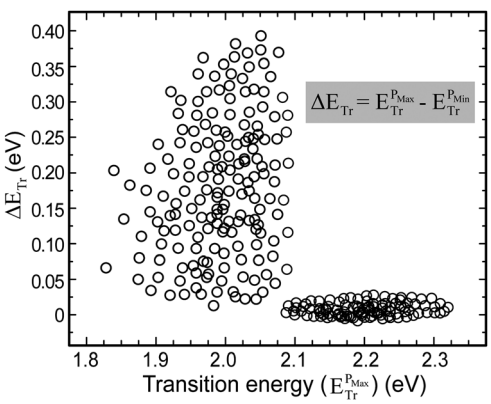

FIG. 4. Scatter plot of difference in transition energies (ΔE_{Tr}) under screened and unscreened conditions as a function of $E_{Tr}^{P_{Max}}$, for 300 individual emission centers.

extremely diverse local polarization field within the emission centers arising from indium compositional fluctuations. The abrupt variation of ΔE_{Tr} at ~2.09 eV is rather surprising; it is possible that even if there is a distribution in size of the red localization centers, there could be a certain critical value below which they do not form bound states. This can set an upper limit to the transition energy for the LLCs which originate from indium compositional fluctuations and hence such an abrupt transition. It is noted that several of the green emission centers do exhibit ΔE_{Tr} of up to ~25 meV (Figure 4) accompanied by slight enhancement (up to ~20%) of emission efficiencies (Figure 3(b)) at very low P_{Ex} (3–20 W cm^{-2}). This suggests the existence of weak polarization fields within these LLCs as well, which is screened even at low carrier concentrations. An alternative explanation could be that the green emission centers are narrower than the red centers along the c-direction, resulting in greater physical confinement and decrease in electron-hole separation.[22] This can dramatically reduce the effect of polarization field and hence, a lack of QCSE.

As a consequence of the large internal polarization fields, LLCs with higher indium mole-fractions display a pronounced ΔE_{Tr} of up to ~400 meV (Figure 4). For nitride based QW heterostructures, such large blue-shifts due to screening of the internal field has not been observed previously. Intriguingly, for the red emission centers, there is no obvious correlation between ΔE_{Tr} and $E_{Tr}^{P_{Max}}$, which is quite surprising because the polarization field is anticipated to increase with higher indium compositions.[16,19] This suggests that the extent of polarization field in the red emitting LLCs depends not only on the local indium mole-fraction, but also on other physical parameter such as size and shape of the nanoscale radiative domains, as well as the amount of strain relaxation therein.[12]

To estimate the intrinsic electric field within nanoscale radiative domains formed due compositional and morphological inhomogeneities, we have solved the self-consistent Schrödinger-Poisson equation for an $In_xGa_{1-x}N$/GaN multiple (5-period) QW system (see supplementary material).[23,27] This calculation shows the existence of an intrinsic electric field of ~4–6 MV/cm, the complete screening of which (i.e., under flat-band conditions) is predicted to result in a spectral blue shift by 600-700 meV. However, ΔE_{Tr} of up to ~400 meV was observed, which translates to polarization field screening by up to ~70% of what is predicted from our calculations. It should be noted that experimentally measured values of ΔE_{Tr} due to QCSE in InGaN alloy based QWs have been consistently found to be much lower than theoretical estimates.[12,19] This has been explained in terms of nonlinear dependency of elastic parameters with increasing indium composition,[24] reduction of the [0001] surface area of localization centers,[12] and the degree of strain relaxation in indium rich centers.[19] For instance, it has been reported that 20%-50% strain relaxation in InGaN heterostructures results in a considerable lowering (by ~400 meV) of the QW transition energies.[25,26]

Alternatively, it is possible that even at P_{Max}, a flat-band condition may not have been achieved, i.e., saturation behavior is observed (Figures 3(a)–3(c)) due to incomplete screening of the internal polarization fields within individual indium-rich emission centers. It is noted that progressive screening of this built-in field with increasing P_{Ex} results in continuous energetic separation between the valence and conduction band. Such a process leads to lowering in the number of available carriers for excitation using the same photon energy. As a consequence, the effective density of delocalized carriers in the QW will *saturate* at a certain P_{Ex}, which may be achieved even with an incomplete screening of the polarization field.

The detrimental effect of the local polarization field on radiative recombination processes is clearly manifested in severely reduced photoemission yields of individual indium-rich LLCs. Under its influence, the light output efficiencies for a large proportion of the red emission centers are quite low, often similar to that of the QW background emission. However, screening of the local built-in field renders these emission centers extremely efficient, considerably more than that of the green emitting centers (Figure 3(b)). This suggests that carrier localization in deep-traps arising from composition related inhomogeneities can result in achieving very high radiative recombination efficiencies in the amber through red spectral regions. Therefore, from this perspective, it can be speculated that deliberate arrangement of indium-rich quantum-disk like domains in QW heterostructures can provide an opportunity to develop $In_xGa_{1-x}N$/GaN based yellow through red emitting LEDs with much higher light-output efficiencies.

In summary, we demonstrate the presence of strong QCSE within spontaneously formed radiative traps in an InGaN QW based green-emitting LED. Blue-shift of transition energies and simultaneous enhancement of radiative efficiencies with increasing carrier density unambiguously reveal the existence of a strong polarization field within individual nanoscale radiative domains. The local polarization field is found to be highly inhomogeneous along in-plane directions of the QWs. Spectrally resolved imaging of two energetically distinct radiative traps reveals that (i) localized luminescent centers arising from indium compositional fluctuations of the active layers can have very strong local polarization fields, and (ii) the built-in field within emission centers related to morphological disorders is relatively less, and as a consequence, it is almost completely screened even at low carrier densities. Importantly, screening of QCSE in indium-rich emission centers results in a blue-shift of transition energies by up to 400 meV, which is much higher than those previously reported (using ensemble measurements) for nitride based QW heterostructures. Finally, our results clearly suggest that the indium mole-fraction within individual emission centers is not solely responsible for the extent of QCSE, and other physical parameters like nanoscale dimensions of the indium rich radiative domains and the degree of strain relaxation therein play a vital role in determining their optoelectronic properties.

We thank K. Bhattacharyya for usage of DST (IRPHA), India funded Centre for Ultrafast Spectroscopy and Microscopy, A. Datta and S. Ghosh for valuable discussions, IIT-Bombay and CSIR (India) for research grants to AC (Scheme: 80(0070)/08/EMR-II) and fellowship to SD, AL, and SB.

[1]S. Pimputkar, J. S. Speck, S. P. DenBaars, and S. Nakamura, Nat. Photonics **3**, 180 (2009).
[2]S. Nakamura, Science **281**, 956 (1998).
[3]N. K. van der Laak, R. A. Oliver, M. J. Kappers, and C. J. Humphreys, Appl. Phys. Lett. **90**, 121911 (2007).
[4]O. Brandt and K. H. Ploog, Nat. Mater. **5**, 769 (2006).
[5]S. Chichibu, T. Azuhata, T. Sota, and S. Nakamura, Appl. Phys. Lett. **69**, 4188 (1996).
[6]F. Bernardini, V. Fiorentini, and D. Vanderbilt, Phys. Rev. B **56**, R10024 (1997).
[7]K. Omae, Y. Kawakami, S. Fujita, Y. Narukawa, and T. Mukai, Phys. Rev. B **68**, 085303 (2003).
[8]K. Okamoto, A. Kaneta, Y. Kawakami, S. Fujita, J. Choi, M. Terazima, and T. Mukai, J. Appl. Phys. **98**, 064503 (2005).
[9]W. Guo, M. Zhang, A. Banerjee, and P. Bhattacharya, Nano Lett. **10**, 3355 (2010).
[10]B. Jochen, R. E. Paul, W. Tao, and W. M. Robert, Appl. Phys. Lett. **98**, 141908 (2011).
[11]S. M. de Sousa Pereira, K. P. O'Donnell, and E. J. da Costa Alves, Adv. Funct. Mater. **17**, 37 (2007).
[12]S. Schulz and E. P. O'Reilly, Phys. Rev. B **82**, 033411 (2010).
[13]H. Schomig, S. Halm, A. Forchel, G. Bacher, J. Off, and F. Scholz, Phys. Rev. Lett. **92**, 106802 (2004).
[14]J. Lähnemann, O. Brandt, C. Pfüller, T. Flissikowski, U. Jahn, E. Luna, M. Hanke, M. Knelangen, A. Trampert, and H. T. Grahn, Phys. Rev. B **84**, 155303 (2011).
[15]F. A. Ponce and D. P. Bour, Nature (London) **386**, 351 (1997).
[16]V. Fiorentini, F. Bernardini, F. D. Sala, A. Di Carlo, and P. Lugli, Phys. Rev. B **60**, 8849 (1999).
[17]S. De, A. Layek, A. Raja, A. Kadir, M. R. Gokhale, A. Bhattacharya, S. Dhar, and A. Chowdhury, Adv. Funct. Mater. **21**, 3828 (2011).
[18]S. De, D. K. Das, A. Layek, A. Raja, M. K. Singh, A. Bhattacharya, S. Dhar, and A. Chowdhury, Appl. Phys. Lett. **99**, 251911 (2011).
[19]U. M. Christmas, A. D. Andreev, and D. A. Faux, J. Appl. Phys. **98**, 073522 (2005).
[20]T. Deguchi, A. Shikanai, K. Torii, T. Sota, S. Chichibu, and S. Nakamura, Appl. Phys. Lett. **72**, 3329 (1998).
[21]J. J. Shi and Z. Z. Gan, J. Appl. Phys. **94**, 407 (2003).
[22]S. Chichibu, T. Sota, K. Wada, and S. Nakamura, J. Vac. Sci. Technol. **16**, 2204 (1998).
[23]S. Dhar, U. Jahn, O. Brandt, P. Waltereit, and K. H. Ploog, Appl. Phys. Lett. **81**, 673 (2002).
[24]O. Ambacher, J. Majewski, C. Miskys, A. Link, M. Hermann, M. Eickhoff, M. Stutzmann, F. Bernardini, V. Fiorentini, V. Tilak, B. Schaff, and L. F. Eastman, J. Phys. D: Condens. Matter. **14**, 3399 (2002).
[25]J. Bai, T. Wang, and S. Sakai, J. Appl. Phys. **90**, 1740 (2001).
[26]L. Guo, X. Wang, H. Xiao, and B. Wang, J. Cryst. Growth **298**, 522 (2007).
[27]See supplementary material at http://dx.doi.org/10.1063/1.4754079 for detail description of experimental techniques and data analyses procedures.

Supplementary Information

Quantum-Confined Stark Effect in Localized Luminescent Centers within InGaN/GaN Quantum-Well Based Light Emitting Diodes

Suman De[1], Arunasish Layek[1], Sukanya Bhattacharya[1], Dibyendu Kumar Das[3], Abdul Kadir[4], Arnab Bhattacharya[4], Subhabrata Dhar[2] and Arindam Chowdhury[1#]*

Details of experimental methods and data analyses procedures

Growth and Characterization of InGaN quantum well light emitting diodes (QW-LED): The epitaxial structures of the samples used in this study are grown on (0001) direction of sapphire substrate by metallorganic vapor phase epitaxy (MOVPE) method in a 3x2 in. close coupled showerhead reactor using trimethylgallium, trimethylindium and ammonia as a precursor. The $In_xGa_{1-x}N$ alloy layer were intended to have a high Indium composition in order to induce higher strain-induced piezoelectric fields and was grown at a relatively low temperature of 660°C and using nitrogen as a carrier gas. The epitaxial structures of this multiple QW-LED consist of a 1.2 µm of n-GaN layer (doping concentration $1x10^{18}/cm^3$) grown on 1.65 µm thick GaN buffer layer. On top of the n-GaN buffer layers, 5-period $In_xGa_{1-x}N$/GaN MQWs were deposited separated by GaN barrier layers. The structural composition and thickness of active layer were estimated by high-resolution X-ray diffraction data which shows distinct superlattice fringes; simulation of the diffraction profiles for multiple reflections shows that active region 4 nm thick $In_{0.22}Ga_{0.78}N$ wells separated by 10nm GaN barrier layers. On top of the active layer, 100 nm thick p-GaN (doping concentration $1x10^{17}/cm^3$) layer was grown. Electroluminescence (EL) spectra obtained from different regions of the sample wafer showed that this was a green emitting working light emitting diodes (LED). Ensemble photoluminescence (PL) spectroscopy was performed using a 405 nm laser, which showed a sharp transition at ~2.6 eV, which is considered to be the quantum well (QW) alloy layer band-gap (see *reference 18* of main manuscript, *Appl. Phys. Lett.* ***99,*** *251911* (2011)).

Spectrally resolved PL Imaging of QWs: Home built spectrally resolved PL microscopy set-up (Figure S1) was used for imaging the 0001 plane of the InGaN heterostructures and interrogate individual localized luminescent centers (LLCs). To avoid overwhelming carrier recombination

through the entire alloy (typical for barrier excitation) which obscures the emission from individual potential traps, carriers were selectively generated in the wells using a tunable 488 nm CW argon ion laser (Melles-Griot CVI) via a 1.49 NA 60X oil immersion objective lens (Nikon). The PL emerging from the sample was collected via the same objective lens in an epi-fluorescence configuration, following which it was allowed to pass through a 496 nm dichroic mirror (Semrock) and a 488 nm notch filter (Semrock), and the eventually imaged through a cooled charge couple device (CCD) camera (DVC 1412AM). Neutral density filters (Thor Labs) were used to control the excitation power density (P_{Ex}) from P_{Min} = 3 Wcm^{-2} to P_{Max} = 1 $kWcm^{-2}$ (measured before the objective lens) which corresponds to carrier concentrations of approximately $5x10^{16}$ to $5x10^{19}$ cm^{-3}, respectively. According to the excitation power density, the exposure times for the CCD camera were varied in order to detect the weakest signals and also avoid detector saturation. To ensure that detection was performed in the linear regimes of the CCD, several power-dependent checks were performed of this as well as other samples; it was observed that the background intensity scaled linearly with excitation power density in the entire regime. The PL intensity images were collected in a 16 bit TIF format, which allowed us to scale the intensities with respect to the CCD exposure times (see Figure 1 of main manuscript) for each excitation power. Semi-quantitative energy mapped images were acquired by superposition of individual intensity images of the same lateral area obtained using two energetic channels (green-yellow: 530-590 nm and orange-red 590-700 nm). The composite images were constructed by quantitative superposition (pixel-by-pixel matching) through either detection channel, which were assigned green and red colors; the resulting pseudo-color intensity images therefore also qualitatively portrayed the transition energies of individual localized luminescent centers (LLCs).

The dispersed PL emission spectra for individual diffraction limited spots were collected in a high-throughput manner using a combination of adjustable slit and transmission grating (70 lines/mm, Optometrics) placed in front of the CCD so as to image both the 0^{th} and 1^{st} order diffraction without moving any part of the setup (see Figure S1). This resulted in simultaneous detection of randomly located individual emission centers and obtaining their spectrally resolved intensity images. The setup was calibrated using four laser wavelengths (488, 514.5, 532 and 633 nm) each time PL spectrum was recorder. A CCD response correction analysis was done for the

spectrally resolved image to obtain an accurate emission profile in the entire energetic range of detection. For long exposures (exceeding 5s), the dark current of the detector was subtracted for spectra to get a corrected intensity signal. The resulting spatially resolved emission spectrum for individual emission centers are fitted with a single Gaussian function to obtain emission maxima (or transitions energies, E_{Tr}), integrated intensity and spectral line width at each excitation powers. To obtain relative PL emission efficiency of individual LLCs with varying power density, the integrated (spectral) intensity of corresponding centers was normalized with respect to the spectral intensities of the surrounding QW background at the corresponding excitation powers. All the data obtained for the red and green emission centers were classified according to their transition energies at P_{Max}.

Time-resolved Photoluminescence microscopy: Fluorescence lifetime imaging microscopy (FLIM) of (In,Ga)N/GaN heterostructures was carried out with a Scanning Confocal Microscope (SCM) set-up using a 470 nm line of pulsed laser excitation with repetition rate of 10 MHz and 250 ps pulse-width. A water immersion objective (60×1.2 NA Olympus) was used to focus the laser to a diffraction limited spot and a 10x10 μm^2 lateral area was raster scanned to obtain PL both intensity and lifetime images in tandem. The two categories of radiative traps (i.e. the green and red emission centers) were first identified from energy-mapped PL intensity images using two detection channels (green-yellow [530-590 nm] and an orange-red [590-700 nm] band pass filters, Semrock), following which the PL lifetime images and single-spot PL decay traces were collected in the absence of any band pass filter. The PL emission was detected through a 20 μm pinhole using a single-photon counting avalanche photodiode. Single-spot PL lifetime decay traces (of individual diffraction-limited spots) were generated by calculating the lifetime of the collected photon counts per pixel using time-correlated single photon counting (TCSPC) technique. Data analyses including de-convolution of instrument response function (IRF, ~250 ps) was carried out using the Symphotime software provided along with the FLIM instrument. The PL decay traces of individual emission centers could not be fit to single-exponential decay; however biexponential decay functions yielded excellent fits. Therefore, a biexponential numerical procedure was used to fit all the decay profiles at three different pump-powers for individual emission centers. Carrier lifetimes (τ) were extracted by averaging the time constants of two components, with their respective weights (following *Principles of Fluorescence*

Spectroscopy by J.R. Lackowicz, 3rd edition). False color intensity weighted lifetime images (shown as calibration bars in Figure 2 of main manuscript) were automatically generated by the data acquisition software (Symphotime), which was exported directly as ASCII files for subsequent data analysis. All measurements were performed at 298K.

Schrodinger-Poisson Calculations: To estimate the intrinsic electric field and their influence on trapped carriers in local potential wells formed due compositional and morphological inhomogeneities, Schrödinger and Poisson equations were solved self-consistently for an $In_xGa_{1-x}N$/GaN multiple QW system. The effect of built-in field on the transition energies of the QWs is estimated by calculating the band profile as a function of indium mole fraction as well as the well-widths of active layers. Note that the screening of the polarization field by the excited carriers is not self-consistently taken into account in this calculation. Values for material parameters like band gap, spontaneous polarization, effective charges and piezoelectric coefficients were obtained following references *Phys. Rev. B.* 56, R10024 (1998) and *J. Appl. Phys.* 89, 5916 (2001), and are shown supplementary Table S1. It is found that the experimentally observed QW transition energy of 2.6 eV (as obtained from large-area PL measurements, *reference 18* of main manuscript, *Appl. Phys. Lett.* 99**,** 251911 (2011)) corresponds to an *average* Indium composition of 18% of *homogeneous InGaN alloy layers*, for a 5-period QW structure with alloy-layer thickness of 4 nm and barrier-widths of 10 nm. In order to estimate the Indium composition in individual red emission centers, it has been assumed that each of these centers act like a QW. Considering that $E_{Tr}^{P_{Min}}$ of the red emission centers corresponds to a completely unscreened situation, the observed $E_{Tr}^{P_{Min}}$ values of 1.6-1.9 eV were used to estimate the amount of Indium in individual red emission centers, which were found to be of 30-32% (*i.e.*~12-14% deviation from average indium composition of the homogeneous alloy). These Indium compositions correspond to an intrinsic polarization field of ~4-6 MV/cm (following *Vegard's Law*: $P_{In_xGa_{1-x}N}^{SP} = P_{InN}^{SP}x + P_{GaN}^{SP}(1-x)$, see Table S1). Now, by fixing the Indium composition for red emission centers in this range, the polarization field is varied to match the observed transition energy at P_{Max} ($E_{Tr}^{P_{Max}}$).The amount of screening was evaluated from shifts in calculated transition energy between the entirely screened (*i.e.* flat-band) and unscreened conditions.

Supplementary Table

Table I. Material parameters of GaN, InN and InGaN for polarization field calculation

Wurtzite structure	**GaN (at 300 K)**	**InN (at 300 K)**	**InGaN**
Bulk band-gap energy (eV)	3.4	0.7	Vegard's law $3.4\,(1-x) + 0.7x - 1.43x\,(1-x)$ Bowing parameter: 3.0
a_0 (Å)[d]	3.189[a]	3.545[a]	
c_0/a_0 (Å)[d]	1.6336[a]	1.627[a]	
e_{33} (C/m^2)[d]	0.73[a]	0.97[a]	
e_{31} (C/m^2)[d]	- 0.49[a]	- 0.57[a]	
c_{13} (GPa)[d]	106[b]	92[b]	
c_{33} (GPa)[d]	398[b]	224[b]	
Relative permittivity ε_r	10.4[c]	14.6[c]	
P^{sp} (Cm^{-2})[e]	-0.029[a]	-0.032[a]	

[a] *Phys. Rev. B.* 56, R10024 (1998)

[b] *J. Appl. Phys.* 89, 5815 (2001)

[c] *Appl. Phys. Lett.* 86, 121915, (2005)

[d] e_{ij} and c_{ij} are the piezoelectric stress coefficients and elastic constants, respectively; a_0 and c_0 are the equilibrium lattice constants for wurtzite structure.

[e] Spontaneous polarization (P^{SP}) of InGaN is calculated using Vegard's law by linear extrapolation as $P^{SP}_{In_xGa_{1-x}N} = P^{SP}_{InN}x + P^{SP}_{GaN}(1-x)$ (in Cm^{-2})

Supplementary Figures

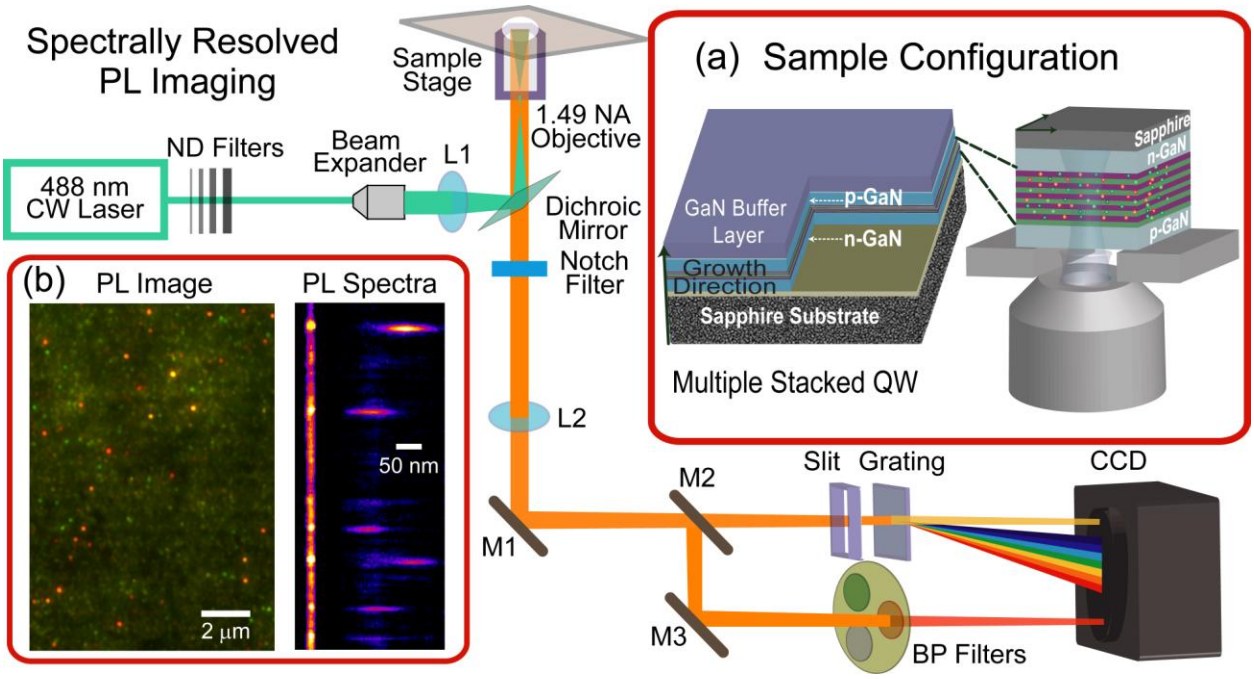

Figure S1. Details of the spectrally-resolved PL microscopy setup; Inset (a) shows a 3D rendition of the MOPVE grown green-emissive InGaN/GaN multiple QW-LED sample grown on the c-place of a sapphire substrate, and the configuration for spectrally resolved PL imaging. Individual emission centers of InGaN/GaN QW were imaged using an oil immersion objective lens (1.49 NA, 60X, Nikon TIRF) by selectively generation carriers in active layer using a 488 nm CW laser. The excitation power density was controlled using a set of neutral density filters. Inset (b) shows a PL intensity image as observed through the microscope eyepiece and the high-throughput collection of single-center PL emission spectra (*see supplementary text*).

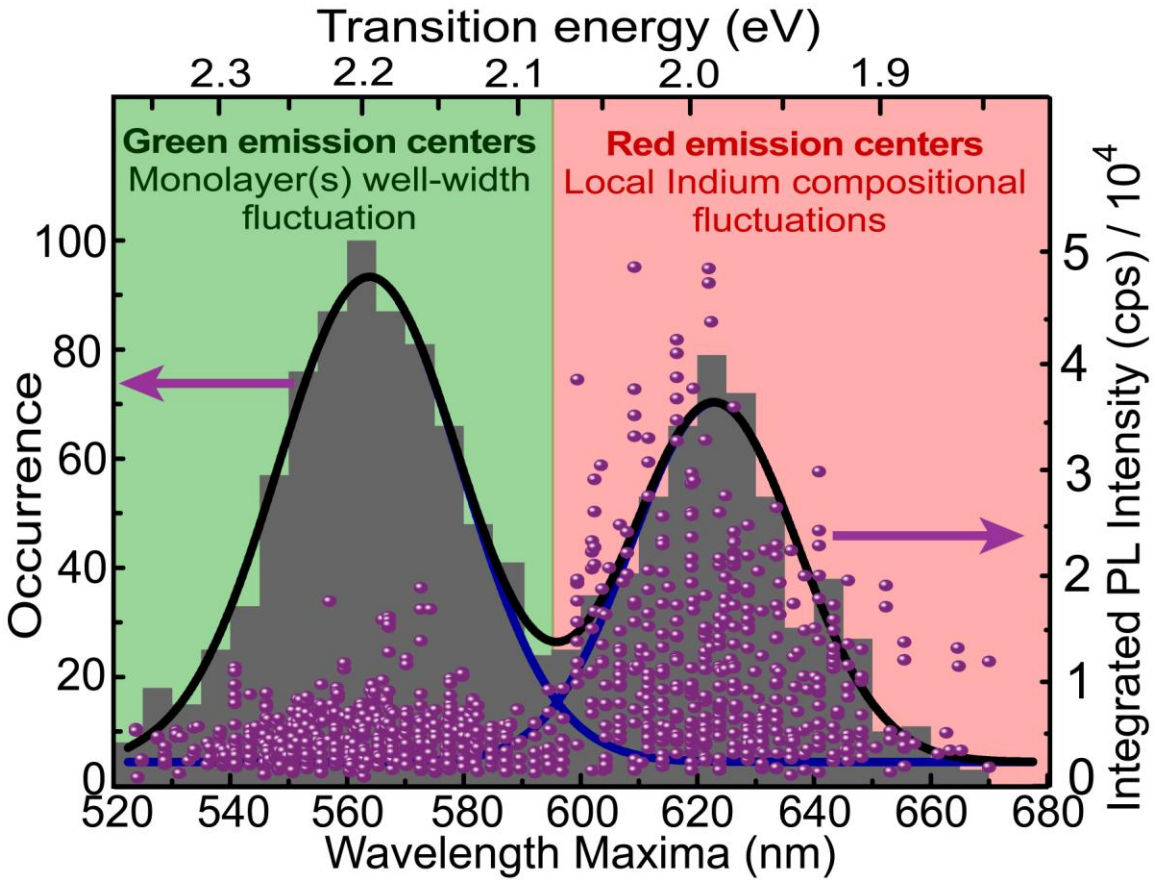

Figure S2. Frequency distribution of single-emission center transition energies (P_{Ex} = 500 W/cm^2 bars) and corresponding integrated PL intensities (spheres) plotted against peak wavelength positions, for 1400 individual LLCs within the same QW-LED sample (adapted from reference 17, *Adv. Func. Mater*. 21, 3828, 2011). The clear bimodal distributions for both E_{Tr} and PL intensities demonstrate that the energetically distinct (E_{Tr} below or above 2.09 eV) radiative traps have different origins. It has been shown previously (References 17 and 18) that emission centers with E_{Tr} lower than 2.09 eV arise from increase of local Indium content within the alloy, while those with E_{Tr} above 2.09 eV originate from interface roughness of the active layers.